Supplemental material for

Strong hybridization driving unusual enhanced negative thermal expansion in $PbTiO_3$-based ferroelectrics

Zhao Pan,[1,2,*] Sergey A. Nikolaev,[2] Xi Shen[1], Takumi Nishikubo,[2,3] Lin Wu,[4] Mengqi Ye,[1] Xubin Ye[1], Shogo Kawaguchi,[6] Yoshihiro Kuroiwa,[4] Richeng Yu[1], Jun Chen,[5,*] Masaki Azuma,[2,3,*] and Youwen Long[1,*]

[1]*Beijing National Laboratory for Condensed Matter Physics, Institute of Physics, Chinese Academy of Sciences, Beijing 100190, China*

[2]*Institute of Integrated Research, Institute of Science Tokyo, 4259 Nagatsuta, Midori, Yokohama, 226-8503, Japan*

[3]*Kanagawa Institute of Industrial Science and Technology (KISTEC), 705-1 Shimoimaizumi, Ebina, Kanagawa 243-0435, Japan*

[4] *Department of Physical Science, Hiroshima University, Higashihiroshima, Hiroshima 739-8526, Japan*

[5]*Beijing Advanced Innovation Center for Materials Genome Engineering and Department of Physical Chemistry*, *University of Science and Technology Beijing, Beijing 100083, China*

[6]*Research and Utilization Division, Japan Synchrotron Radiation Research Institute (JASRI), SPring-8, 1-1-1 Kouto, Sayo-cho, Sayo-gun, Hyōgo 679-5198, Japan*

[*]E-mail: zhaopan@iphy.ac.cn; junchen@ustb.edu.cn; mazuma@msl.titech.ac.jp; ywlong@iphy.ac.cn

To gain further insight into the hybridization of $0.6PbTiO_3$-$0.4BiCoO_3$ and $0.5PbTiO_3$-$0.5BiFeO_3$ from a microscopic perspective, we carry out electronic structure calculations. We begin by considering $BiCoO_3$ and $BiFeO_3$ in the tetragonal structure and analyze the Co-O and Fe-O bond hybridization. It is worth noting that although the room-temperature phase of $BiFeO_3$ is classed as rhombohedral (*R3c* space group), we adopt the tetragonal structure to investigate the difference in Fe-O and Co-O hybridization in the same environment. Electronic structure calculations were performed using the GGA+*U* method with effective Hubbard parameters of U_{eff} = 4.0 and 6.0 eV, which fall within the typical range for such systems [2-4]. We utilized a $2 \times 2 \times 2$ supercell with three types of antiferromagnetic configurations imposed on Co and Fe sites, as shown in Figure S7. The Brillouin zone was sampled by a $6 \times 6 \times 6$ *k*-point mesh, and the crystal structures were optimized with a total force convergence criterion of 10^{-4} eV/Å.

The results are summarized in Table S3 and Supplementary Figures S7-S9. The calculated Co-O1 bond lengths are found to be shorter than the Fe-O1 bond lengths. As follows from the densities of states in Figure S8, the hybridization between the 3*d* and O 2*p* states is markedly different owing to the distinct electronic configurations of Co^{3+} and Fe^{3+}. In the case of a more electronegative Co^{3+}, the 3*d* electrons experience a stronger pull narrowing the gap with the O *p* states and extending their overlap, which results in higher covalency of the Co-O1 bond. In contrast, the energy mismatch between the Fe *d* and O *p* states is found to be larger than that of Co, rendering the Fe-O1 bond less covalent compared to the Co-O bond, as further evidenced in the calculated partial charge densities shown in Figure S9.

The results obtained for $BiCoO_3$ and $BiFeO_3$ are consistent with the trends observed in $0.6PbTiO_3$-$0.4BiCoO_3$ and $0.5PbTiO_3$-$0.5BiFeO_3$. To investigate hybridization within the experimental structures, electronic structure calculations were performed using $2 \times 2 \times 5$ and $2 \times 2 \times 2$ supercells, respectively, as shown in Figure S4. In these calculations, random disorder was introduced alongside an antiferromagnetic configuration for the Fe and Co ions. An effective Hubbard parameter of U_{eff} = 4.0 eV was applied to both systems, and the Brillouin zone was sampled using $6 \times 6 \times 2$ and $6 \times 6 \times 5$ *k*-point meshes for the Co- and Fe-based systems, respectively.

The results summarized in Figures S5 and 5 reveal features similar to those of $BiFeO_3$ and $BiCoO_3$ and align well with the findings from the Maximal Entropy Method (MEM). Ultimately, our first-principles calculations serve to qualitatively support the MEM results. While the latter can

be considered more beneficial as disorder is accounted for statistically without needing to explicitly model all possible atomic configurations, the results of electronic structure calculations provide a detailed microscopic perspective on the local density of states and hybridization that can potentially underpin the enhanced NTE properties.

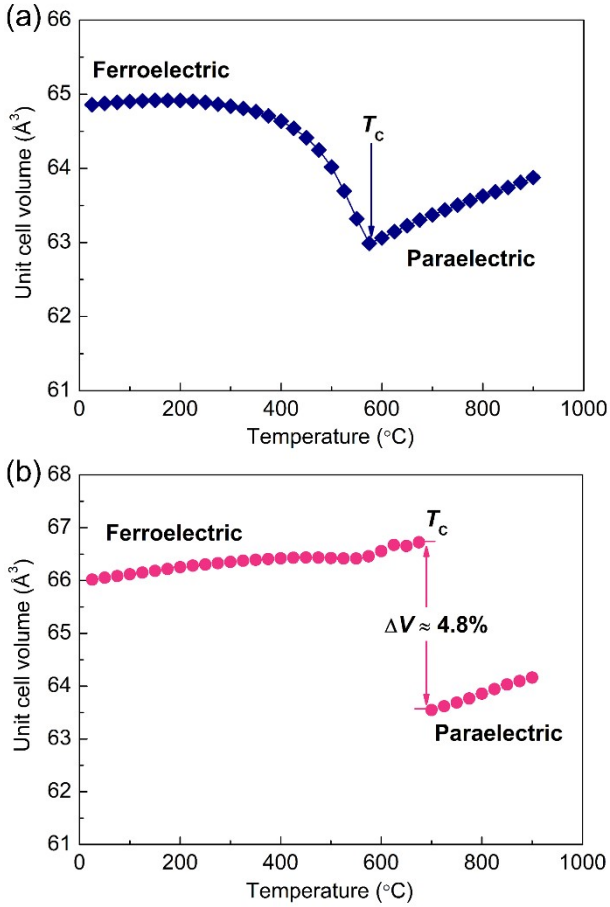

Figure S1. Temperature-dependence of the unit cell volume for (a) 0.7PT-0.3BC and (b) 0.5PT-0.5BC, respectively.

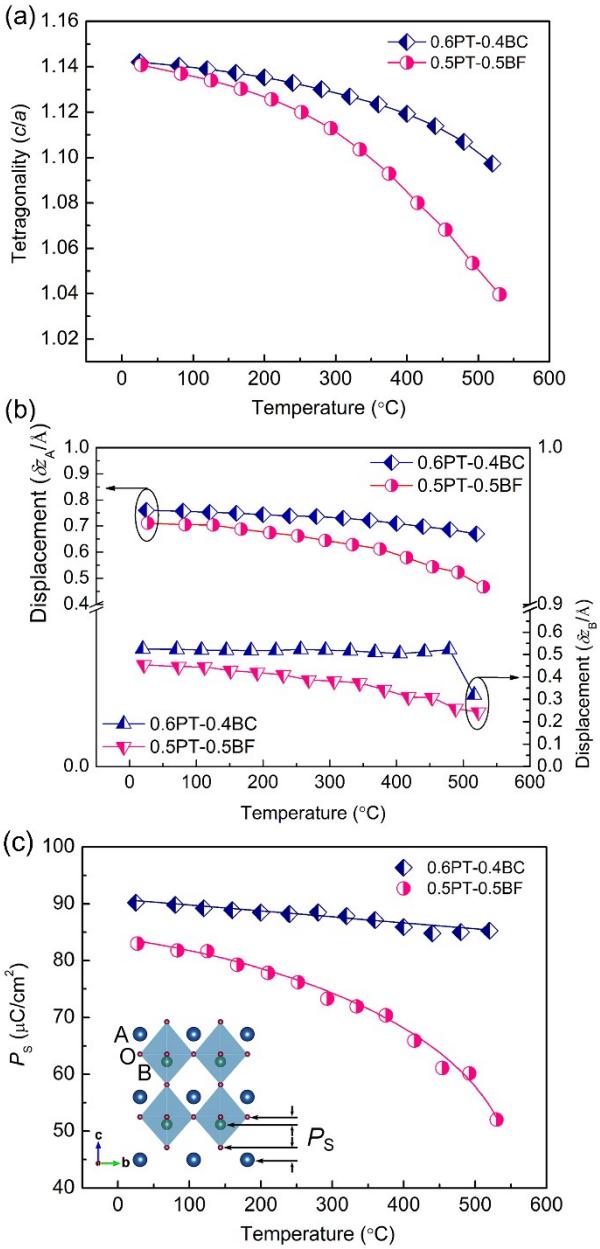

Figure S2. Temperature dependence of (a) *c*/*a* ratio, (b) spontaneous polarization displacement of the A-site (δz_A) and B-site (δz_B), and (c) ferroelectric spontaneous polarization P_S for 0.5PT-0.5BF and 0.6PT-0.4BC, respectively. The inset is the schematic diagram of P_S.

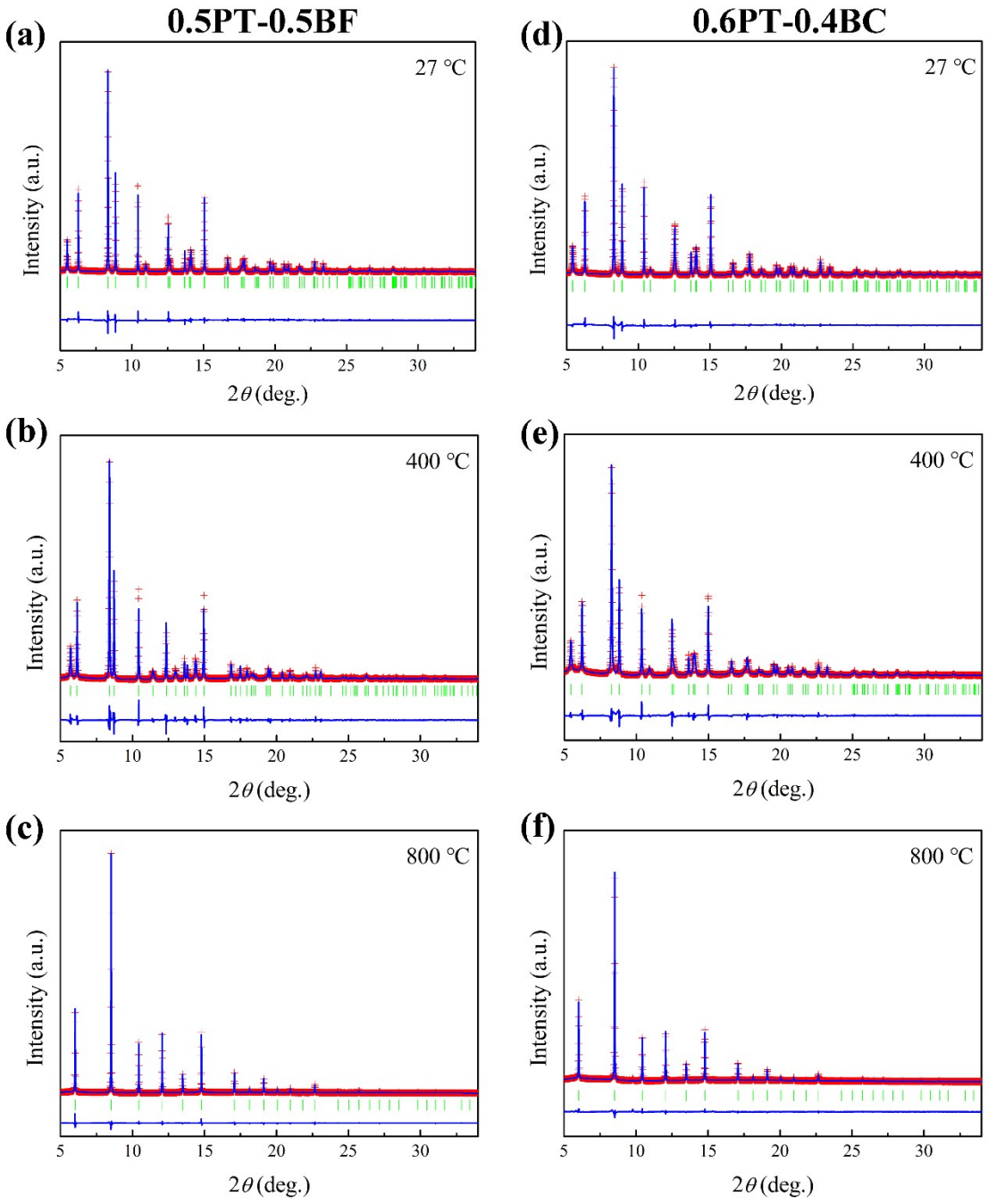

Figure S3. Rietveld full profile refinements of SXRD patterns of 0.5PT-0.5BF and 0.6PT-0.4BC at tetragonal ferroelectric ((a, d) 27 ºC, (b, e) 400 ºC) and (c, f) cubic paraelectric (800 ºC), respectively. Observed (red, solid circles), calculated (black line), and their difference profiles (bottom line) are shown. The Bragg reflection positions are indicated by the green ticks.

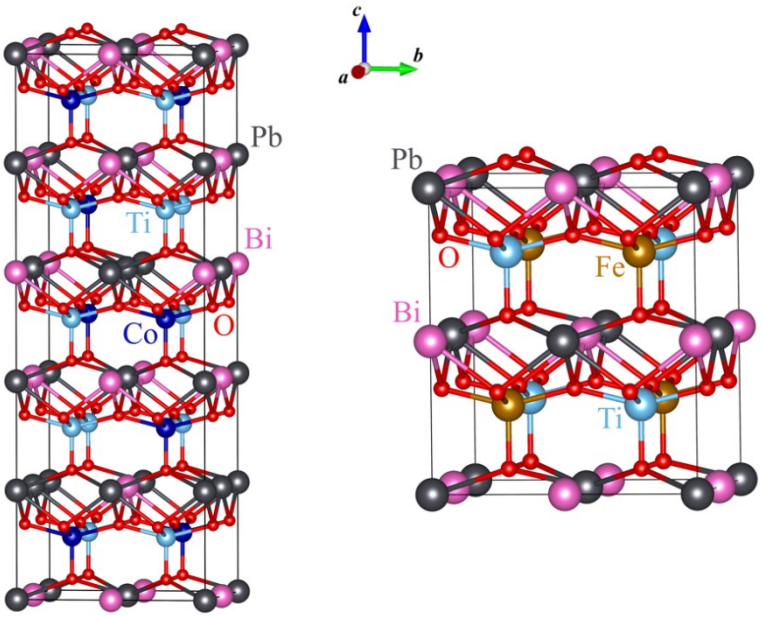

Figure S4. Supercells of $0.6PbTiO_3$-$0.4BiCoO_3$ ($2 \times 2 \times 5$, left) and $0.5PbTiO_3$-$0.5BiFeO_3$ ($2 \times 2 \times 2$, right) used in electronic structure calculations.

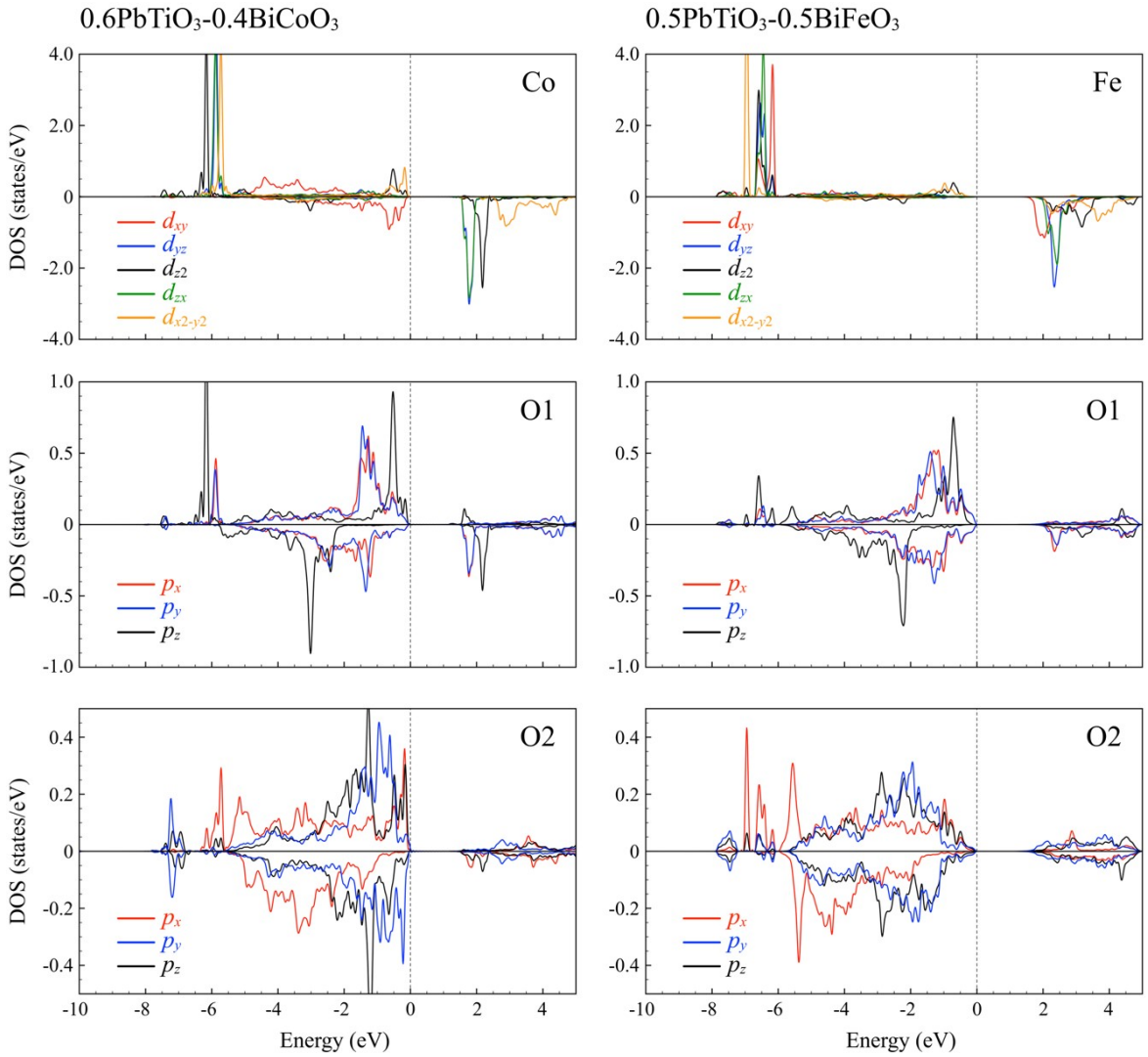

Figure S5. Density of states (DOS) obtained for $0.6PbTiO_3$-$0.4BiCoO_3$ (left) and $0.5PbTiO_3$-$0.5BiFeO_3$ (right). The densities of states are shown for individual atoms within a single $(Co/Fe)O_5$ pyramid. Positive and negative values correspond to the spin-up and spin-down states, respectively. The results are obtained for experimental crystal structures at 27 K.

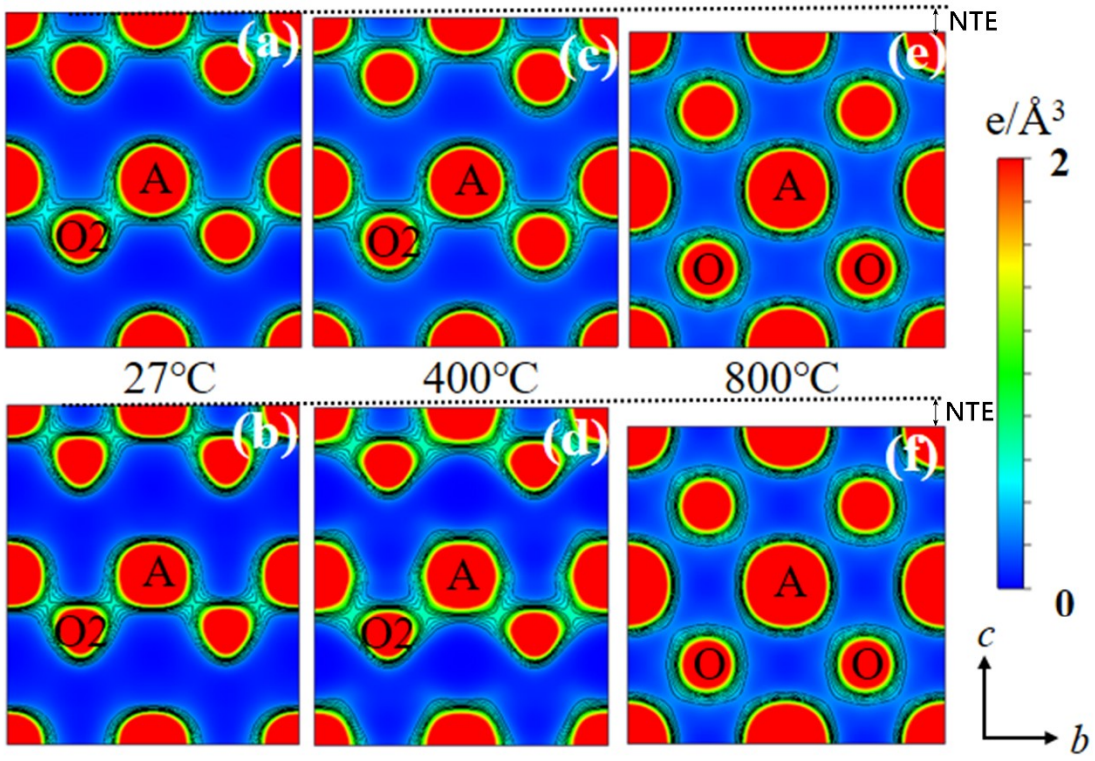

Figure S6. Elelctron-density distributions on the *bc* planes of tetragonal ferroelectric 0.5PT-0.5BF ((a) 27 ºC and (c) 400 ºC) and 0.6PT-0.4BC ((b) 27 ºC and (d) 400 ºC) and cubic paraelectric 0.5PT-0.5BF ((e) 800 ºC) and 0.6PT-0.4BC ((f) 800 ºC) from synchrotron diffraction data. Contours from 0 to 2 $Å^{-3}$ by 0.2 $Å^{-3}$ step in (a)-(f). The dashed line indicates the role of spontaneous polarization (δ_A) in NTE.

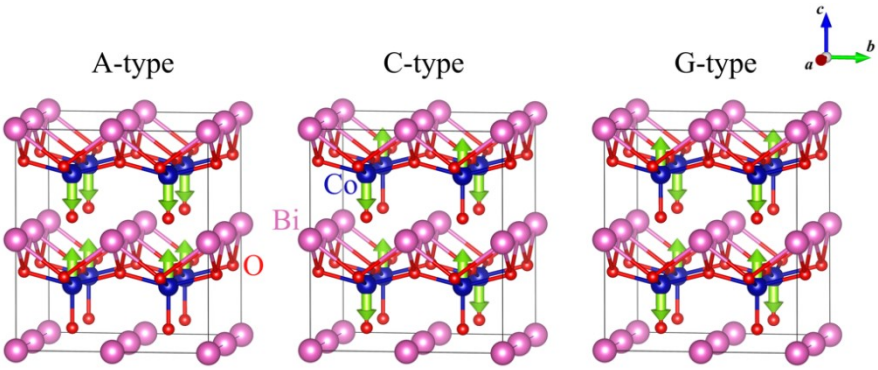

Figure S7. Antiferromagnetic configurations in tetragonal $BiCoO_3$ and $BiFeO_3$ on a $2 \times 2 \times 2$ supercell.

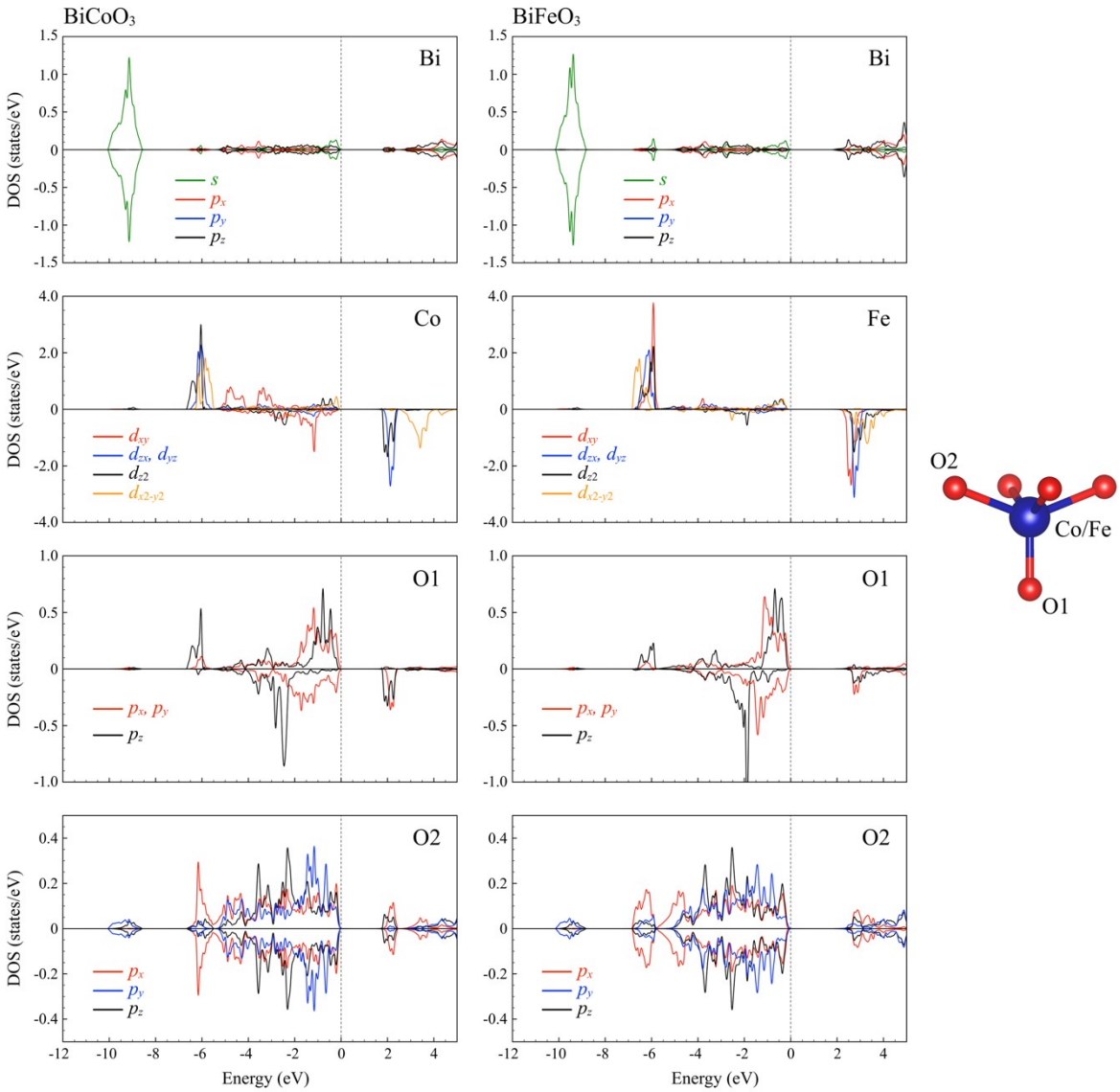

Figure S8. Density of states (DOS) obtained for $BiCoO_3$ (left) and $BiFeO_3$(right) from GGA+U calculations (U_{eff} = 4.0 eV) and the C-type antiferromagnetic configuration. The densities of states are shown for individual atoms within a single (Co/Fe)O_5 pyramid. Positive and negative values correspond to the spin-up and spin-down states, respectively.

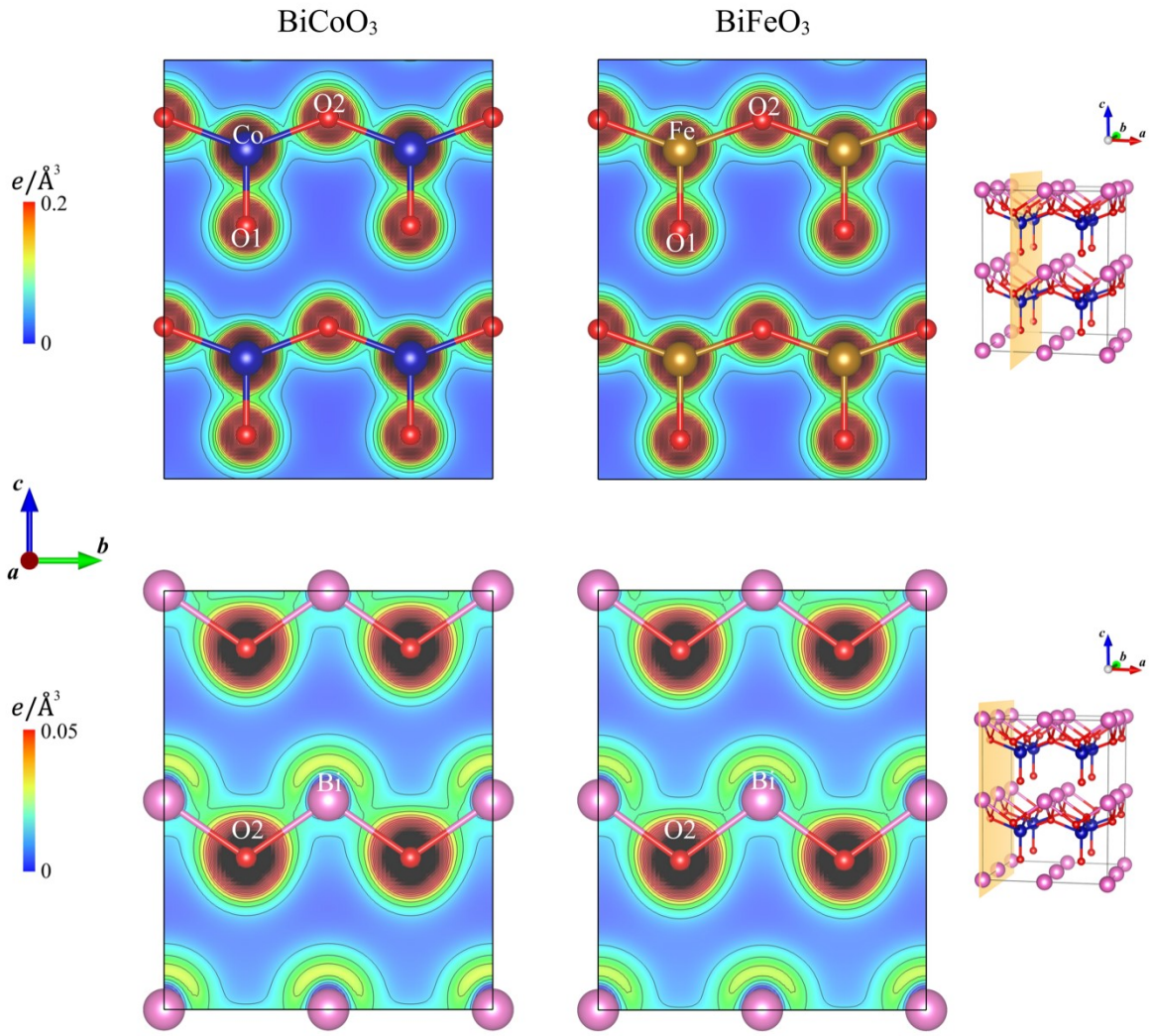

Figure S9. Partial charge densities of $BiCoO_3$ (left) and $BiFeO_3$(right) obtained from GGA+U calculations (U_{eff} = 4.0 eV) and the C-type antiferromagnetic configuration. Charge densities are calculated in the energy window of [-8.0, 0.0] eV with respect to the Fermi level. Contours are plotted with intervals of 0.03 and 0.01 $e/Å^3$ for the top and bottom panels, respectively.

Table S1. Refined structural parameters of the 0.5PT-0.5BF compound at 27 °C, 400 °C, and 800 °C, respectively.

Composition	Space group	Atom	Site	g	*x*	*y*	*z*	*B*(Å^2)
0.5PT-0.5BF	*P*4*mm*(27°C)[a]	Pb	1a	0.5	0	0	0	1.66(1)
		Bi	1a	0.5	0	0	0	1.66(1)
		Ti	1a	0.5	0.5	0.5	0.5604(2)	0.38(3)
		Fe	1a	0.5	0.5	0.5	0.5604(2)	0.38(3)
		O1	1a	1.0	0.5	0.5	0.1443(3)	1.99(5)
		O2	2c	1.0	0.5	0	0.6681(8)	0.65(7)
	*P*4*mm*(400°C)[b]	Pb	1a	0.5	0	0	0	2.84(4)
		Bi	1a	0.5	0	0	0	2.84(4)
		Ti	1a	0.5	0.5	0.5	0.5593(2)	1.22(1)
		Fe	1a	0.5	0.5	0.5	0.5593(2)	1.22(1)
		O1	1a	1.0	0.5	0.5	0.1056(4)	4.40(7)
		O2	2c	1.0	0.5	0	0.6340(3)	2.01(4)
	Pm-3*m*(800°C)[c]	Pb	1a	0.5	0	0	0	6.15(6)
		Bi	1a	0.5	0	0	0	6.15(6)
		Ti	1b	0.5	0.5	0.5	0.5	2.11(7)
		Fe	1b	0.5	0.5	0.5	0.5	2.11(7)
		O	3c	1.0	0.5	0	0.5	3.41(0)

[a]space group *P*4*mm*, Z = 1, $a = b$ = 3.8483(5) Å, c = 4.3928 (7) Å, *R*-factor: R_{wp} = 9.46%, R_p = 6.92%. [b]space group *P*4*mm*, Z = 1, $a = b$ = 3.9043(7) Å, c = 4.2167 (8) Å, *R*-factor: R_{wp} = 6.90%, R_p = 4.22%. [c]space group *Pm*-3*m*, Z = 1, a = 3.9973(2) Å, *R*-factor: R_{wp} = 3.07%, R_p = 4.74%.

Table S2. Refined structural parameters of the 0.6PT-0.4BC compound at 27 °C, 400

°C, and 800 °C, respectively.

Composition	Space group	Atom	Site	g	*x*	*y*	*z*	*B*(Å2)
0.6PT-0.4BC	*P*4*mm*(27°C)[a]	Pb	1a	0.6	0	0	0	1.40(2)
		Bi	1a	0.4	0	0	0	1.40(2)
		Ti	1a	0.6	0.5	0.5	0.5578(3)	0.45(9)
		Co	1a	0.4	0.5	0.5	0.5578(3)	0.45(9)
		O1	1a	1.0	0.5	0.5	0.1694(6)	1.23(8)
		O2	2c	1.0	0.5	0	0.6706(7)	0.98(5)
	*P*4*mm*(400°C)[b]	Pb	1a	0.6	0	0	0	2.12(1)
		Bi	1a	0.4	0	0	0	2.12(1)
		Ti	1a	0.6	0.5	0.5	0.5686(3)	0.86(1)
		Co	1a	0.4	0.5	0.5	0.5686(3)	0.86(1)
		O1	1a	1.0	0.5	0.5	0.1586(9)	7.98(5)
		O2	2c	1.0	0.5	0	0.6589(1)	1.76(7)
	Pm-3*m*(800°C)[c]	Pb	1a	0.6	0	0	0	5.46(2)
		Bi	1a	0.4	0	0	0	5.46(2)
		Ti	1b	0.6	0.5	0.5	0.5	2.34(6)
		Co	1b	0.4	0.5	0.5	0.5	2.34(6)
		O	3c	1.0	0.5	0	0.5	2.85(7)

[a]space group *P*4*mm*, Z = 1, $a = b = 3.8534(6)$ Å, $c = 4.4034(9)$ Å, *R*-factor: $R_{wp} = 5.42\%$, $R_p = 3.38\%$. [b]space group *P*4*mm*, Z = 1, $a = b = 3.8652(7)$ Å, $c = 4.4172\ (8)$ Å, *R*-factor: $R_{wp} = 5.74\%$, $R_p = 3.68\%$. [c]space group *Pm*-3*m*, Z = 1, $a = 4.0004(4)$ Å, *R*-factor: $R_{wp} = 3.41\%$, $R_p = 10.77\%$.

Table S3 Results of electronic structure calculations for tetragonal $BiCoO_3$ and $BiFeO_3$: energy per formula unit (with respect to the ground state); magnetic moment at the B site; B-O1, B-O2, and A-O2 bond lengths; the lattice constants.

	Energy, eV/f.u.	Magnetic moment, μ_B	B-O1, Å	B-O2, Å	A-O2, Å	a, Å	c, Å
	$BiCoO_3$, U_{eff} = 4.0 eV						
A-type	0.128	3.050	1.733	2.033	2.278	3.774	4.803
C-type	0	2.977	1.747	2.013	2.289	3.757	4.782
G-type	0.016	2.985	1.747	2.012	2.290	3.759	4.781
	$BiCoO_3$, U_{eff} = 6.0 eV						
A-type	0.094	3.181	1.733	2.023	2.286	3.774	4.763
C-type	0	3.123	1.742	2.008	2.292	3.760	4.754
G-type	0.013	3.131	1.743	2.008	2.292	3.761	4.752
	$BiFeO_3$, U_{eff} = 4.0 eV						
A-type	0.126	4.216	1.824	2.016	2.317	3.771	4.815
C-type	0	4.139	1.839	1.999	2.326	3.757	4.803
G-type	0.008	4.144	1.841	1.998	2.328	3.760	4.789
	$BiFeO_3$, U_{eff} = 6.0 eV						
A-type	0.091	4.387	1.831	2.003	2.325	3.770	4.774
C-type	0	4.323	1.842	1.992	2.331	3.758	4.770
G-type	0.005	4.328	1.845	1.990	2.333	3.761	4.756

.